

Paraelectric-resonance study of KCl:CN^-

F. Holuj

*University of Windsor, Windsor, Ontario, Canada
and University of California, Santa Cruz, California 95064*

Frank Bridges

University of California, Santa Cruz, California 95064

(Received 7 December 1978; revised manuscript received 17 April 1979)

A paraelectric-resonance study has been made of KCl:CN^- over the frequency range 32–74 GHz for electric fields up to 275 kV/cm. The data can be fitted to a $\langle 111 \rangle$ -dipole model. The tunneling parameters (in GHz) are: $\eta = -19.45$ ($\pm 2\%$), $\mu = +1.7$ ($\pm 10\%$), and $\nu = -0.23$ ($\pm 50\%$). These parameters give the zero-field splitting: 32.55, 38.45, and 46.15 GHz. The electric-dipole moment is $p = 0.53$ D ($\pm 2\%$). The new tunneling parameters open the question as to the sign of the tunneling parameters.

I. INTRODUCTION

CN^- is one of the few paraelectric-paraelastic centers in alkali halides that has a very small electric-dipole moment. It has been investigated by various methods, amongst the most recent of which are: high-resolution ir spectroscopy,¹ phonon spectroscopy,² Raman spectroscopy,³ and birefringence studies.⁴ None of these methods, however, used electric fields in excess of 100 kV/cm.⁴ Rather, the dipole orientations have been deduced from the stress data. In particular, a study¹ by ir of KCl:CN^- subjected to stress clarified that the orientation of the dipoles appears to be along the $[111]$ direction (or the so-called $\langle 111 \rangle$ model). A number of subsequent investigations successfully explained their results using this model and found the alternate $\langle 100 \rangle$ model, which served as basis for interpretations of earlier data, not adequate.

In the present experiment we have examined the paraelectric resonance (PER) spectra of KCl:CN^- in the presence of electric fields of up to 275 kV/cm. This represents the highest electric field used in paraelectric studies to date. The purpose of this study was to determine which model fits the PER data best and to determine its parameters with greater accuracy than those available in the literature. It will be remembered that the PER method is superior for accomplishing this task since it measures directly such quantities as the zero-field splitting (ZFS) and the uncorrected electric-dipole moment (of the CN^- ion in the KCl host in this case).

The paper is organized as follows: Section II presents a theoretical background in which we summarize the formulas which are used in the analysis part (Sec. V). Sections III and IV describe the experimental results. Finally in Sec. VI we discuss our

new results and how they relate to the recent literature on the KCl:CN^- system.

II. THEORETICAL BACKGROUND

A. Models

The substitutional CN^- ion replaces Cl^- in KCl and likely sits somewhat off-center in this host since the observed electric-dipole moment is considerably larger than the moment observed for CN^- in KBr and KI.⁵ Consequently, both an intrinsic moment (of the CN^- ion) and an off-center dipole moment must exist. However, in view of the many experiments which have been explained using simple models (with only dipole moment) and the lack of any strong evidence for two different dipole moments from the paraelectric resonance experiments (as observed for KI:OH^-),⁶ we will consider only the simplest models at this time.

Two different approaches have been used to describe the paraelectric centers and have been discussed in detail previously. One is the hindered rotator model which is particularly useful when transitions to upper excited states are considered.⁷ The other is the tunneling model, which considers only the lowest multiplet of energy levels and ignores additional excited states.⁸ Since the observed PER transitions are assumed to arise solely within the ground-state multiplet, we will use this model to analyze our data.

The tunneling model is best described using the directed basis states which are the eigenstates in the presence of large electric fields. Each state represents the dipole oriented along one of a set of equivalent axes within the crystal. All other dipole orientations are not permitted within the ground state and therefore dipole energies in the presence of an electric

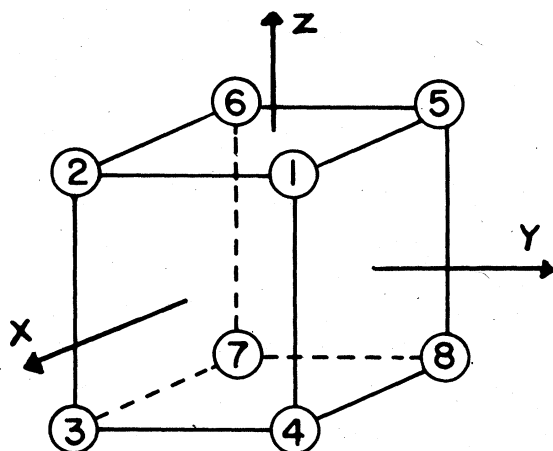


FIG. 1. Directed state labeling for the $\langle 111 \rangle$ dipole model. The dipole is assumed to be at the center of the cube pointing towards one of the balls.

field will be quantized. To restrict the dipole orientation to a few directions, a multiwell potential is assumed which has minima along the equivalent symmetry axes. The eigenstates of the system then correspond to the dipole moment occupying one or more of these potential wells. The symmetry of this potential also must be consistent with the symmetry of the host lattice and must therefore have O_h symmetry for the cubic KCl lattice. The three simplest models⁸ for cubic crystals are the $\langle 100 \rangle$ model with six minima along the $\langle 100 \rangle$ axes, the $\langle 111 \rangle$ model with eight minima along the $\langle 111 \rangle$ axes, and the $\langle 110 \rangle$ model with twelve minima along the $\langle 110 \rangle$ axes. The model of interest for CN^- is $\langle 111 \rangle$, whose directed dipole states are indicated in Fig. 1. Here one should picture the dipole as occupying the center of the cube and pointing towards one of the numbered balls.

In the limit of very high potential barriers between the minima, the potential wells are isolated from each other and the system is eightfold degenerate. However, for finite barriers, some tunneling of the dipole from one potential well to another occurs and lifts the eightfold degeneracy in a manner consistent with the cubic symmetry of the host lattices. A phenomenological model has been developed to describe such systems in terms of tunneling matrix elements.⁸ Three tunneling parameters are necessary for the $\langle 111 \rangle$ model: the nearest-neighbor (70.5°) tunneling, second-nearest-neighbor (109.5°) tunneling, and 180° tunneling. These parameters are defined in terms of the directed states (given in Fig. 1) as follows:

$$\begin{aligned} \eta(70.5^\circ) &= \langle 1|H_c|2\rangle = \langle 1|H_c|5\rangle = \dots, \\ \mu(109.5^\circ) &= \langle 1|H_c|3\rangle = \langle 1|H_c|6\rangle = \dots, \\ \nu(180^\circ) &= \langle 1|H_c|7\rangle = \langle 2|H_c|8\rangle = \dots, \end{aligned}$$

where H_c is the crystal-field Hamiltonian. The resulting 8×8 matrix for H_c is tabulated in the Appendix.

If we now add an electric field \vec{E} (whose direction with respect to the crystal shall be indicated as a subscript; e.g., $E_{[111]}$ denotes an electric field along the crystallographic $[111]$ direction), the energy levels are split further (see Fig. 2). The additional term in the Hamiltonian is the interaction of the electric-dipole moment, \vec{p} with \vec{E} , or

$$H_E = -\vec{p} \cdot \vec{E}. \quad (1)$$

The diagonal terms which Eq. (1) introduces for the $\langle 111 \rangle$ system are given in Eq. (A2). For convenience, we have also included in the Appendix the eigenvalues of the matrix H_c [Eq. (A3)] and the difference between the neighboring levels for dom-

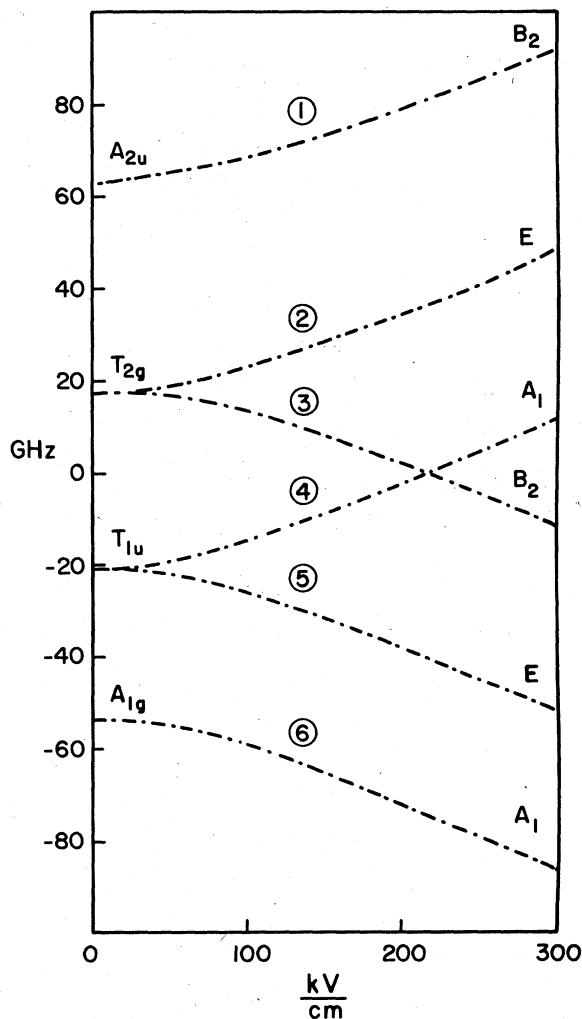


FIG. 2. Energy levels of the tunneling multiplets obtained using the parameters in Table I for the model $\langle 111 \rangle$ for $E_{[100]}$. The labeling of levels is according to the irreducible representation of O_h and C_{4v} point groups.

inant η [Eq. (A4)].

Finally we remind the reader that random strains are invariably present in the crystal samples and can play an important role in the interpretation of the PER spectra since the coupling to random internal strain⁹ is one of the main broadening mechanisms. For $\langle 111 \rangle$ dipole systems, only the T_{2g} component of stress couples to the paraelastic dipole; this means that the compressional stress along the $[100]$ axis does not affect the spectra.⁹ Consequently, one might expect that samples cut for $E_{[100]}$ studies might have somewhat narrower absorption lines. As will be seen in Sec. IV these lines are indeed narrower compared to the $E_{[111]}$ and $E_{[110]}$ data.

III. APPARATUS AND EXPERIMENTAL PROCEDURE

A. Spectrometer

The microwave spectrometer and the associated electronics used throughout this research have been described elsewhere.¹⁰ The study of the CN^- ion by the PER method, however, requires an *unusually* large electric field. To meet this requirement the sample and the electrodes were introduced inside the resonant microwave cavity as shown in Fig. 3. The electrode (3) which was made of 1 mm thick copper sheet had its edges carefully rounded and a groove cut to receive the connecting wire from the choke. No soldering was permitted as it usually introduced dirt and roughness to the surface through which electric discharges may occur. An important innovation, however, was the introduction of a 0.002-in. Mylar sheet between the sample (1) and the electrode (3). It covered the entire cavity to within 1 mm of the walls. This location quite effectively prevented electrical discharges at 4.2 K but was less effective at 1.5° K. The rf choke (8) was wrapped with at least two layers of similar Mylar sheet.

B. Sample preparation

Most samples were prepared from a single-crystal boule grown at the Crystal Growth Laboratory of the

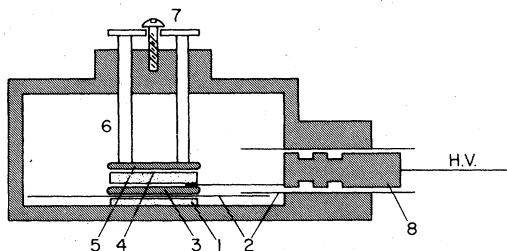


FIG. 3. Experimental arrangement inside the resonant cavity. 1. Sample. 2. Mylar sheets. 3. Electrode. 4. Quartz plate. 5. Suppressor. 6. Quartz capillary tubing. 7. Spring. 8. Choke.

University of Utah, Salt Lake City, and doped in the melt with KCN. An estimated molar concentration of CN^- was 8×10^{-5} . A qualitative measurement designed to check for concentration effects, if any, was also done using samples cut from a boule having 10^{-3} molar concentration of CN^- . We shall henceforth refer to this sample as the "concentrated sample."

The crystal wafers, sawed off the boule with a wet string saw, were first oriented along either the (100), (111), or (110) planes using an especially constructed jig as the holder in the x-ray diffractometer. They were then lapped on a damp cloth so that the finished wafer was accurately oriented along the chosen plane. The accuracy of this orientation is estimated to be within 0.5° . Many such samples had to be prepared since electrical "discharges" over a crystal sample resulted in its destruction. One sample rarely lasted for more than one run.

The thickness of the samples varied: One group, used for experiments involving intense electric fields, was 0.025 cm thick (as measured with a dial gauge) and had an area of the order of 1 cm^2 . Another group had thicknesses of 0.041 cm and 0.079–0.089 cm. They were used whenever the 0.025 cm samples gave poor resonances (due mainly to broadening or low-signal intensity).

We did not anneal any samples although some samples were heated to 450–500°C in a Li^+ thermal diffusion experiment. The PER resonances of CN^- were not notably affected thereafter, but the Li^+ signals, also present in untreated samples, were enhanced.

The intensity of the electric field was calculated using the geometry of the arrangement shown in Fig. 3. The dielectric constant of the Mylar sheet was assumed to be $\epsilon_m = 3$ and that of KCl, $\epsilon_x = 5.0$. The electric field was calculated using the formula

$$E = V / (l_x + l_m \epsilon_x / \epsilon_m) \quad (2)$$

where V is the applied voltage, and l_x and l_m are the thicknesses of the sample and the Mylar sheet, respectively. l_x was measured with a dial gauge. We used the Li^+ signal (when it was visible) both as a qualitative check of the electric field intensity and as an indicator of the spectrometer sensitivity. Unfortunately, this signal invariably vanished after the sample had been subjected to an intense electric field.

Most experiments described in this paper were performed at 4.2° K. Some spectra for $E_{[100]}$ were examined at 1.5° K, but they were difficult to deal with because of the electrical breakdown which takes place in liquid He below the λ point.

IV. EXPERIMENTAL RESULTS

We present in Figs. 4–6 the trace recordings of the PER resonances for the applied electric fields $E_{[100]}$,

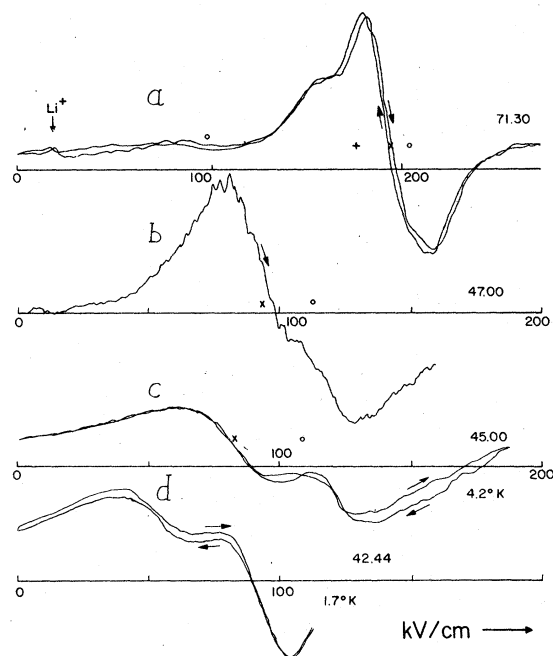


FIG. 4. Trace recording of PER spectra for $E_{[100]}$. Arrows indicate the direction of E sweep. See Fig. 8 for labeling of lines. (a) four resonances whose location are marked by circles and crosses and a small Li^+ signal. A simulation of the main three resonances by Gaussians is shown in Fig. 7(a). (b) and (c) two resonances at low E field at 4.2°K ; they illustrate the variation in the shape and intensity of resonances obtained from two different samples (and two different cavity modes). (d) A trace obtained at 1.7°K showing reversal of intensity when compared with (c). (c) and (d) were obtained using the same sample.

$E_{[110]}$, and $E_{[111]}$, respectively. The sample thicknesses were (in cm): 0.0267, 0.041, 0.044, and 0.044 (for $E_{[100]}$); 0.040 and 0.047 (for $E_{[110]}$), and 0.044 and 0.038 (for $E_{[111]}$). The frequencies (in GHz) are indicated on each trace. Excepting the one trace at 1.7°K all others were taken at 4.2°K .

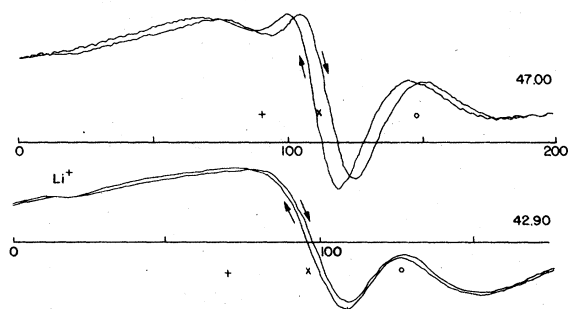


FIG. 5. Trace recording of PER spectra for $E_{[110]}$. The two traces were obtained from two different samples at 4.2°K . A simulation of the upper trace by three Gaussians is shown in Fig. 7(c).

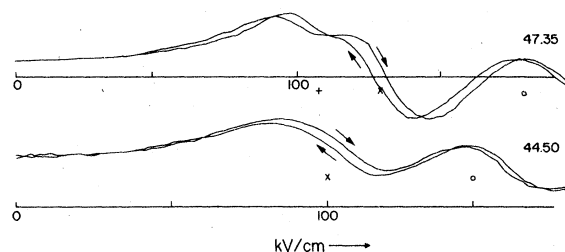


FIG. 6. Trace recording of PER spectra for $E_{[111]}$. The two traces were obtained from two different samples of 4.2°K . A simulation of the upper trace by three Gaussians is shown in Fig. 7(b).

Owing to their excessive width and their complexity these spectra were very difficult to analyze. To aid the analysis the following was done: double trace each resonance with increasing and decreasing electric fields (arrows in Figs. 4–6); when necessary, trace the resonances several times; reject any traces when they showed excessive noise or poor resolution.

The positions of the resonances were estimated by comparing the data with sets of theoretical curves, samples of which are shown in Fig. 7. Here each curve approximately simulates the top curves of Figs. 4–6.

For three lines, the derivative of the Gaussian line shape is given by the expression

$$f(X) = \sum_{i=1}^3 \frac{A_i}{2} \frac{X - X_i}{\sigma_i^3} \exp\left[-\frac{1}{2} \left(\frac{X - X_i}{\sigma_i}\right)^2\right], \quad (3)$$

where A_i , X_i , and σ_i are, respectively, the intensity, the center, and the width of the Gaussians. Figure 7 shows the component Gaussians (thin lines) as well as their sum (thick line). The A_i values (which are proportional to the area under the Gaussian in question) are given in the caption.

The plots of frequency versus the electric field of the PER spectra for each field orientation are shown in Figs. 8–10. The symbols (circles and crosses) occurring in Figs. 8–10 and in Figs. 4–6 correspond with each other.

Here are some more general observations relating to the spectra:

(i) The width of the lines, and therefore, the resolution, varied to some extent from sample to sample (especially for the 0.025 cm samples).

(ii) The hysteresis associated with the direction of the sweep also varied. (There is some evidence that this is somehow connected with the Mylar sheet.)

(iii) Two runs for $E_{[100]}$ and one run for $E_{[110]}$ using the concentrated sample duplicated all the major features of the spectrum (and exhibited the expected concentration broadening).

(iv) The electric field was calculated using Eq. (2). This procedure gave self-consistent values for E as is

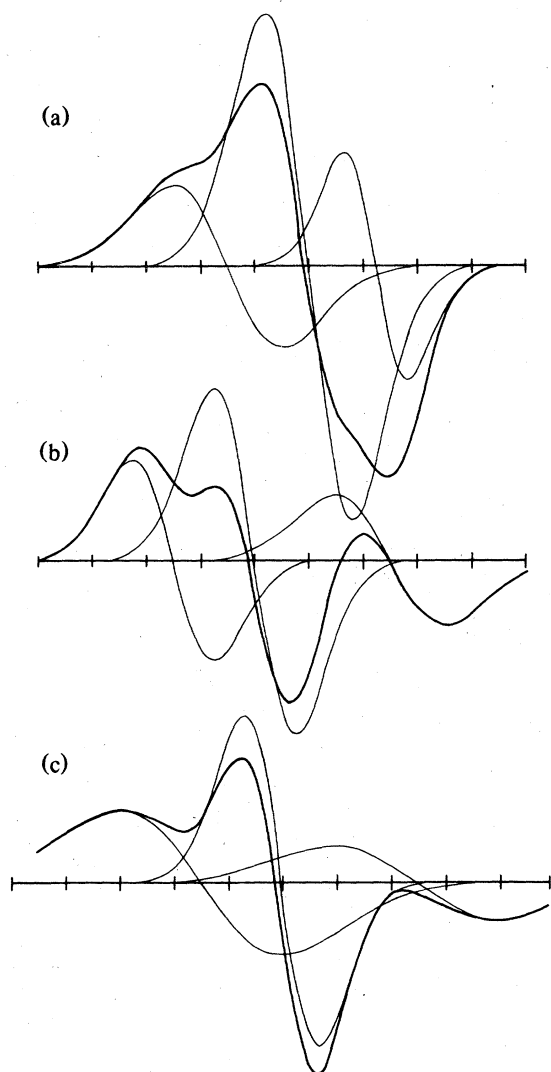


FIG. 7. Simulation of experimental line shapes by three Gaussians whose amplitude ratios are: 2:4:1 (a), 1:1.7:1.1 (b), and 1:2:2 (c). The Gaussians are represented by thin lines and their resultant by a thick line. The three line shapes simulate, respectively, the signals in Figs. 4, 6, 5.

evident from the experimental points in Fig. 8, which were obtained using a diversity of sample thicknesses. In most cases a sheet of Mylar was present, but in some runs we replaced the Mylar with a mica sheet. Also when the field was low enough (<100 kV/cm) no isolating dielectric sheet was present.

(v) A search was made for zero-field resonances which were found at two frequencies: 32.5 and 37.5 GHz.

(vi) At some frequencies it was not possible to locate all the resonances. In such cases these resonances are missing in Figs. 8–10 (but their presence may be deduced from measurement at neighboring

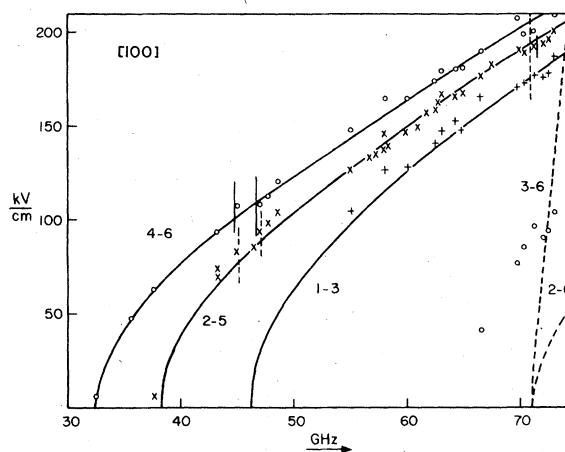


FIG. 8. Experimental data (points) and predicted resonances for (111) model whose parameters appear in Table I (lines) for $E_{[100]}$. The lines are labeled according to the scheme of Fig. 2. The 3-6 and 2-6 lines represent forbidden transitions. The vertical lines indicate the estimated widths of those resonances which also appear in Fig. 4 (4.2° K case only).

frequencies).

(vii) For $E_{[100]}$ (Fig. 8), the separation between the three main resonances decreases with the E field and only one slope is observed. For $E_{[110]}$ and $E_{[111]}$ the lines converge asymptotically to one slope also.

(viii) For $E_{[100]}$ the lines with ZFS at 32.5 and 37.5 GHz are resolved at low frequencies [see Figs. 4(c) and 4(d)]. At 4.2° K the low-field line (which

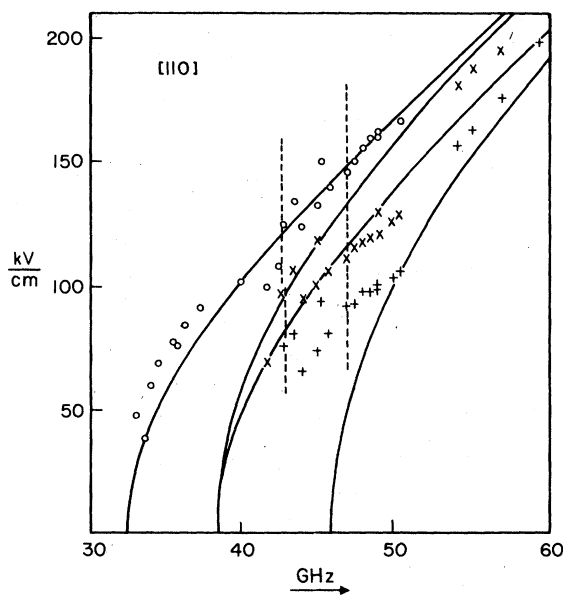


FIG. 9. Experimental data and predicted resonances for $E_{[110]}$ (see Fig. 8 for more details). The vertical lines indicate the widths of the resonances appearing also in Fig. 5.

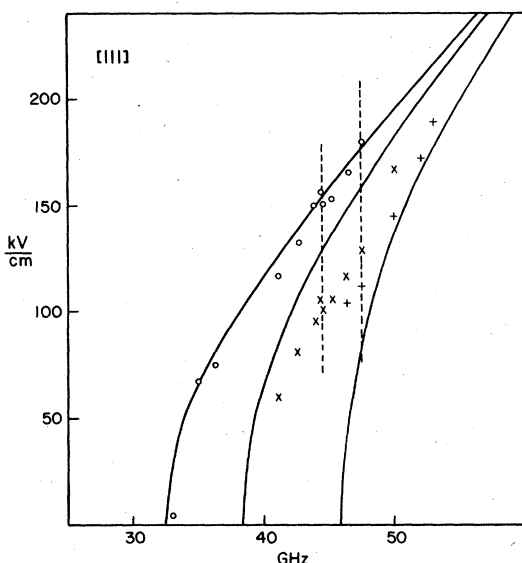


FIG. 10. Experimental data and predicted resonances for $E_{[111]}$ (see Fig. 8 for more details). The vertical lines indicate the widths of the resonances appearing also in Fig. 6.

corresponds to the 2-5 transition and which is marked by an \times) has a larger intensity than the high-field one (4-6 transition which is indicated by a circle). At 1.7° K [Fig. 4(d)] these intensities are reversed. We shall return to this point below.

V. ANALYSIS

Using the computer program based on the theory outlined in Sec. II, we obtained the set of allowed resonance lines which give the best rms fit of the experimental data for $E_{[100]}$ and also have large transition probabilities. The resulting values for the dipole moment and the tunneling parameters are listed in Table I and the theoretical curves are shown in Figs.

TABLE I. Parameters of the tunneling spectrum of CN⁻ in KCl at 4.2° K from the PER data. (In GHz when applicable.)

p	η	μ	ν
0.53 D \pm 2%	-19.45 \pm 2%	+1.70 \pm 10%	-0.23 \pm 50%
Ordering of levels (GHz)			
A_{1g}	T_{1u}	T_{2g}	A_{2u}
-53.48	-20.93	17.53	63.68

8-10. In addition to matching the two ZFS at 32.5 and 38.5, the analysis also gave a third ZFS at 46.2 GHz. These parameters were then used to predict the resonances for $E_{[110]}$ and $E_{[111]}$ (Figs. 9 and 10, respectively).

The fit for $E_{[110]}$ and $E_{[111]}$ could not be improved by including the electrostriction effect or by adopting an alternate $\langle 110 \rangle$ model. The latter does give a good fit for $E_{[100]}$ with dominant second-neighbor tunneling [so called $\mu(90^\circ)$ parameter] but fits to the $E_{[111]}$ and $E_{[110]}$ data are even worse than for the $\langle 111 \rangle$ model. In any case, because of the excessive widths, the fit at these crystal orientations cannot be expected to be particularly good. It should be noted in Figs. 9 and 10 that many experimental points fall between the theoretical lines. This is what would be expected if two resonances of nearly equal intensity and breadth were not resolved. These data served the sole purpose of definitely eliminating the alternative $\langle 110 \rangle$ model.

There is one weak and broad resonance which appears at frequencies above 66 GHz in Fig. 8, and is indicated by a circle in Fig. 4(a). It does not seem to fit the simple $\langle 111 \rangle$ model. In an effort to explain its existence we included T_{2g} random strains. This produced two very weak lines in the vicinity of the experimental points, but the intensity was still several orders of magnitude too low (dashed lines in Fig. 8). Further, the 3-6 line (see Fig. 2 for transition labeling) predicted by the model is extremely steep and therefore would be too broad to be observed experimentally. If this line arises from CN⁻, it may correspond to higher-energy levels of the system. Without additional evidence this line must remain unidentified.

With η as the dominant tunneling parameter, the dominant line will be the middle transition (3-4) as observed but a clear identification of the other two lines which belong to the transitions (1-3) and (4-6) was not obtained from the 4.2 K data alone. However, the changes in the $E_{[100]}$ spectra as the temperature is lowered from 4.2 to 1.7 K provide a clear criterion for identification. As discussed under point 8, Sec. IV, the changes in intensity at these two temperatures indicate that the high-field line must originate from the ground-state level. Hence the assignment of transitions must be made as indicated in Fig. 8.

This conclusion rests on the following argument. It is a peculiarity of the $\langle 111 \rangle$ model with dominant η parameter that the frequency spectrum is independent of the sign of μ . Although it is not particularly obvious, this fact is true for all electric fields (as can be proved by extending the calculation of the allowed transitions back to zero electric field). Since the allowed transitions are between the neighboring energy levels [see the Appendix, Eq. (A4)], the line 4-6 (for $\mu = 1.7$, Fig. 8) becomes 1-3 for $\mu = -1.7$ (and vice

versa). The above observation of relative intensities, however, eliminated the $\mu = -1.7$ GHz case. (The same swapping of resonances occurs also for $E_{[110]}$ and $E_{[111]}$.)

VI. DISCUSSION

In this section we review the recent results (since 1974) of investigations of KCl:CN by other methods and compare our data with these earlier investigations.

a. Raman scattering. The CN^- stretching vibration (2089 cm^{-1}) using 4880 \AA radiation was studied.³ An attempt was made, using the various Raman configurations, to observe the pure tunneling transitions that accompany the main stretching mode; the rationale being that the $A_{1g} \rightarrow T_{2g}$ and $T_{1u} \rightarrow A_{2u}$ transitions of the $\langle 111 \rangle$ model should appear in the T_{2g} geometry. Other Raman configurations do not lead to any resolved transitions. Experimentally, a pair of lines, separated by 4.8 cm^{-1} , appeared in the T_{2g} geometry and no structure appeared in the E_g geometry. According to Eq. (3) and a single-parameter $\langle 111 \rangle$ model, this separation equals 8η and gives $\eta = 0.6\text{ cm}^{-1}$. The presence of the small μ and ν parameters would not lead to any measurable effect.

b. High-resolution ir spectroscopy. In this experiment the same CN^- stretching mode (2089 cm^{-1}) was studied under conditions of externally applied stress and electric field.¹ Of particular interest to us are the results obtained under the application of stress.

In the case of stress $S_{[111]}$ (applied along the $[111]$ direction) the separation between the outer pair of Stokes-anti-Stokes lines for E_{\parallel} polarization increases rapidly for small values of $S_{[111]}$ and then it levels off for larger $S_{[111]}$ (see Fig. 8, Ref. 1). A single-parameter $\langle 111 \rangle$ model with $\eta = -18.9\text{ GHz}$ predicts a somewhat smaller separation. Referring to Table I the new parameters, by giving several zero-field split-

tings, actually improve the agreement with experiment. In the case of the inner pair (for E_{\perp} polarization) the situation is similar and improvement with experiment results. The reason for this improvement can be traced to Fig. 2, where it is seen, for $\vec{E} = 0$, that the levels of T_{1u} and T_{2g} have moved down by 0.17 cm^{-1} (5.1 GHz approximately) in relation to A_{1g} and A_{2u} .

We mention in passing the "soft" $\langle 111 \rangle$ model introduced in Ref. 1 to account for the behavior of the system under $S_{[100]}$ stress (a behavior which a rigid $\langle 111 \rangle$ model could not predict). The gist of this postulate is that the η parameter is slightly stress dependent and becomes larger for tunneling between potential wells that are brought closer together by the stress and smaller for those cases in which the wells are moved apart by stress. For the PER results, the good agreement between theory and experiment for $E_{[100]}$ using the rigid $\langle 111 \rangle$ model suggests that there is no electrical analog to this soft model for fields below 275 kV/cm .

c. Finally we mention two additional studies of KCl:CN⁻: electro-birefringence studies⁴ and phonon spectroscopy.² In the former, the Kerr effect for $E_{[100]}$ was found to be much smaller than for $E_{[111]}$ and thus indicated unequivocally that the model must be $\langle 111 \rangle$. The latter agreed with this determination of the orientation and provided a second estimate of the largest tunneling parameter: $\eta = -21.1\text{ GHz}$.

The PER results are in essential agreement with the earlier measurements, and provide an accurate measurement of the dipole moment. This small (uncorrected) moment p_u is difficult to measure and a value of 0.5 Debye has been estimated from dielectric studies.^{5,11} However, measurements of p_u by this method do require a knowledge of the CN^- concentration and would not yield a very reliable number. Our determination of this moment, $p_u = 0.53$ Debye, is however in agreement with the dielectric measurements.^{5,11}

The PER measurements clearly indicate three

TABLE II. Relative intensities of PER lines for $E = 120\text{ kV/cm}$ and for the two choices $\mu = \pm 1.7$ GHz. The experimental data are for the traces shown in Fig. 4(c) (4.2° K) and Fig. 4(d) (1.7° K); their accuracy probably lies within 25% error. All values are relative to the 2-5 transition.

Transition	$\mu = -1.7$		$\mu = +1.7$		Experiment	
	4.2° K	1.5° K	4.2° K	1.5° K	4.2° K	1.7° K
2-5 (Middle)	1	1	1	1	1	1
4-6 (High field)	0.25	0.1	0.6	1.3	0.5	1

TABLE III. Predicted and measured relative intensities of the spectrum in Fig. 4(a) (at 71.3 GHz). Approximate experimental error is noted.

μ (GHz)	-1.7	+1.7	Experiment
1-3 (Low field)	1.17	0.45	0.5 \pm 25%
2-5 (Middle field)	1	1	1.0 \pm 15%
4-6 (High field)	0.24	0.53	0.3 \pm 50%

separate tunneling splittings and, consequently, to explain them on an energy-level diagram, we require the presence of different ZFS's. For the $\langle 111 \rangle$ model this means that the second- and third-nearest-neighbor tunneling parameters cannot be neglected. Our results for η , μ , and ν (Table I) compare well with those obtained from ir studies¹ ($\eta = -18.9$ GHz) and from phonon resonance studies² ($\eta = -21.1$ GHz). The magnitude of μ is close to the limit of 1.2 GHz estimated in Ref. 1.

However, to have the observed temperature dependence of the relative intensities, the experimental line with ZFS of 32.5 GHz must be identified as the 4-6 transition. This corresponds to a *positive* value for the second-nearest-neighbor tunneling parameter, $\mu = +1.7$ GHz. (This is the first evidence that the small tunneling parameters may be positive, although in the literature they are always assumed to be negative.) A quantitative examination of the intensities in question is presented in Table II. Here we see that for $\mu = -1.7$ GHz, the high-field line (or 4-6) at 1.5° K is smaller by an order of magnitude than that obtained either experimentally or for $\mu = 1.7$ GHz. Table II also shows that the experimental intensities of both lines and those for $\mu = 1.7$ GHz agree quite well.

Table III presents the theoretical and experimental analysis of the intensities of the spectrum in Fig. 4(a) (for 71.30 GHz). We find here that for $\mu = -1.7$ GHz the predicted intensity of the low-field line is much larger than for the experimental. (The latter being quite close to the value for $\mu = +1.7$ GHz.) The high-field line (last row of Table III) gives a value lying closer to that for $\mu = -1.7$. However, since this line is poorly resolved for all frequencies above 55 GHz (at which band a full three-line spectrum is measurable), its experimental intensity remains uncertain (hence the large error margin for this row).

Finally, we remark that there is no fundamental objection against a positive value for a minor tunneling parameter. The principal parameter (η in our case) must, of course, be negative to ensure that the

ground-energy state belongs to the A_{1g} representation of the O_h group (or equivalently, that its wave function must not contain any nodes¹²). Also, our case does not seem to be unique. A preliminary examination of the PER of KBr:Li⁺ indicates that here, too, some positive minor parameters fit the experimental data best.¹³

ACKNOWLEDGMENTS

One of us (F.H.) wishes to thank the Natural Sciences and Engineering Research Council of Canada for a travel grant and the University of Windsor, Ontario, Canada, for financial support in the form of a sabbatical leave. This work was supported in part by a grant from the NSF.

APPENDIX

The matrix of the crystal-field Hamiltonian, H_c , in the approximation of noninteracting dipoles and nonoverlapping of states for the $\langle 111 \rangle$ system is

$$H_c = \begin{pmatrix} 1 & 2 & 3 & 4 & 5 & 6 & 7 & 8 \\ 0 & \eta & \mu & \eta & \mu & \eta & \nu & \mu \\ 0 & \eta & \mu & \mu & \eta & \mu & \nu & \mu \\ 0 & \eta & \nu & \mu & \eta & \mu & \nu & \mu \\ 0 & \mu & \nu & \mu & \eta & \mu & \nu & \mu \\ 0 & \eta & \mu & \eta & \mu & \eta & \nu & \mu \\ 0 & \eta & \mu & \eta & \mu & \eta & \nu & \mu \\ 0 & \eta & \mu & \eta & \mu & \eta & \nu & \mu \\ 0 & \eta & \mu & \eta & \mu & \eta & \nu & \mu \end{pmatrix} \quad (A1)$$

The dipolar diagonal elements are

$$\begin{aligned} D_1 &= \frac{-p}{\sqrt{3}}(E_x + E_y + E_z), & D_2 &= \frac{-p}{\sqrt{3}}(E_x - E_y + E_z), \\ D_3 &= \frac{-p}{\sqrt{3}}(E_x - E_y - E_z), & D_4 &= \frac{-p}{\sqrt{3}}(E_x + E_y - E_z), \\ D_5 &= \frac{-p}{\sqrt{3}}(-E_x + E_y + E_z), & D_6 &= \frac{-p}{\sqrt{3}}(-E_x - E_y + E_z), \\ D_7 &= \frac{-p}{\sqrt{3}}(-E_x - E_y - E_z), & D_8 &= \frac{-p}{\sqrt{3}}(-E_x + E_y - E_z). \end{aligned} \quad (A2)$$

When Eq. (A1) is diagonalized it gives the following energy levels:

$$\begin{aligned} E(A_{1g}) &= 3\eta + 3\mu + \nu, & E(T_{1u}) &= \eta - \mu - \nu, \\ E(T_{2g}) &= -\eta - \mu + \nu, & E(A_{2u}) &= -3\eta + 3\mu - \nu. \end{aligned} \quad (A3)$$

The differences between the neighboring levels are

$$\begin{aligned} E(T_{1u}) - E(A_{1g}) &= -2\eta - 4\mu - 2\nu, \\ E(T_{2g}) - E(T_{1u}) &= -2\eta + 2\nu, \\ E(A_{2u}) - E(T_{2g}) &= -2\eta + 4\mu - 2\nu. \end{aligned} \quad (A4)$$

- ¹H. U. Beyeler, Phys. Rev. B 11, 3078 (1975).
²R. Windheim, Solid State Commun. 18, 1183 (1976).
³D. Durand and F. Lüty, Phys. Status Solidi B 69, 63 (1975).
⁴A. Diaz-Gongora and F. Lüty, Phys. Status Solidi B 86, 127 (1978).
⁵M. S. Sack and M. C. Moriarty, Solid State Commun. 3, 93 (1965).
⁶W. M. Kelly and F. Bridges, Phys. Rev. B 18, 4606 (1978).
⁷H. U. Beyeler, Phys. Status Solidi B 52, 419 (1972).
⁸M. Gomez, S. P. Bowen, and J. A. Krumhansl, Phys. Rev. 153, 1009 (1967).
⁹A. S. Nowick and W. R. Heller, Adv. Phys. 12, 251 (1963).
¹⁰F. Bridges, Rev. Sci. Instrum. 45, 130 (1974).
¹¹P. P. Peressini, J. P. Harrison, and R. O. Pohl, Phys. Rev. 182, 939 (1969).
¹²L. D. Landau and E. M. Lifshitz, *Quantum Mechanics* (Addison-Wesley, London, 1958), p. 56.
¹³R. J. Russell, Ph.D. thesis (University of California, 1978) (unpublished).